



Development of limited-view tomography for measurement of Spray G plume direction and liquid volume fraction

Lukas Weiss^{1,2} · Michael Wensing^{1,2} · Joonsik Hwang³ · Lyle M. Pickett³ · Scott A. Skeen³

Received: 10 October 2019 / Revised: 13 December 2019 / Accepted: 9 January 2020 / Published online: 27 January 2020
© The Author(s) 2020

Abstract

The method for direct injection of fuel in the cylinder of an IC engines is important to high-efficiency and low-emission performance. Optical spray diagnostics plays an important role in understanding plume movement and interaction for multi-hole injectors, and providing baseline understanding used for computational optimization of fuel delivery. Traditional planar or line-of-sight diagnostics fail to capture the liquid distribution because of optical thickness concerns. This work proposes a high-speed (67 kHz) extinction imaging technique at various injector rotations coupled to computed tomography (CT) for time-resolved reconstruction of liquid volume fraction in three dimensions. The number of views selected and processing were based on synthetic (modeled) liquid volume fraction data where extinction and CT adequately reconstructed each plume. The exercise showed that for an 8-hole, symmetric-design injector (ECN Spray G), only three different views are enough to reproduce the direction of each plume, and particularly the mean plume direction. Therefore, the number of views was minimized for experiments to save expense. Measurements applying this limited-view technique confirm plume–plume variations also detected with mechanical patternation, while providing better spatial and temporal resolution than achieved previously. Uncertainties due to the limited view within pressurized spray chambers, the droplet size, and optically thick regions are discussed.

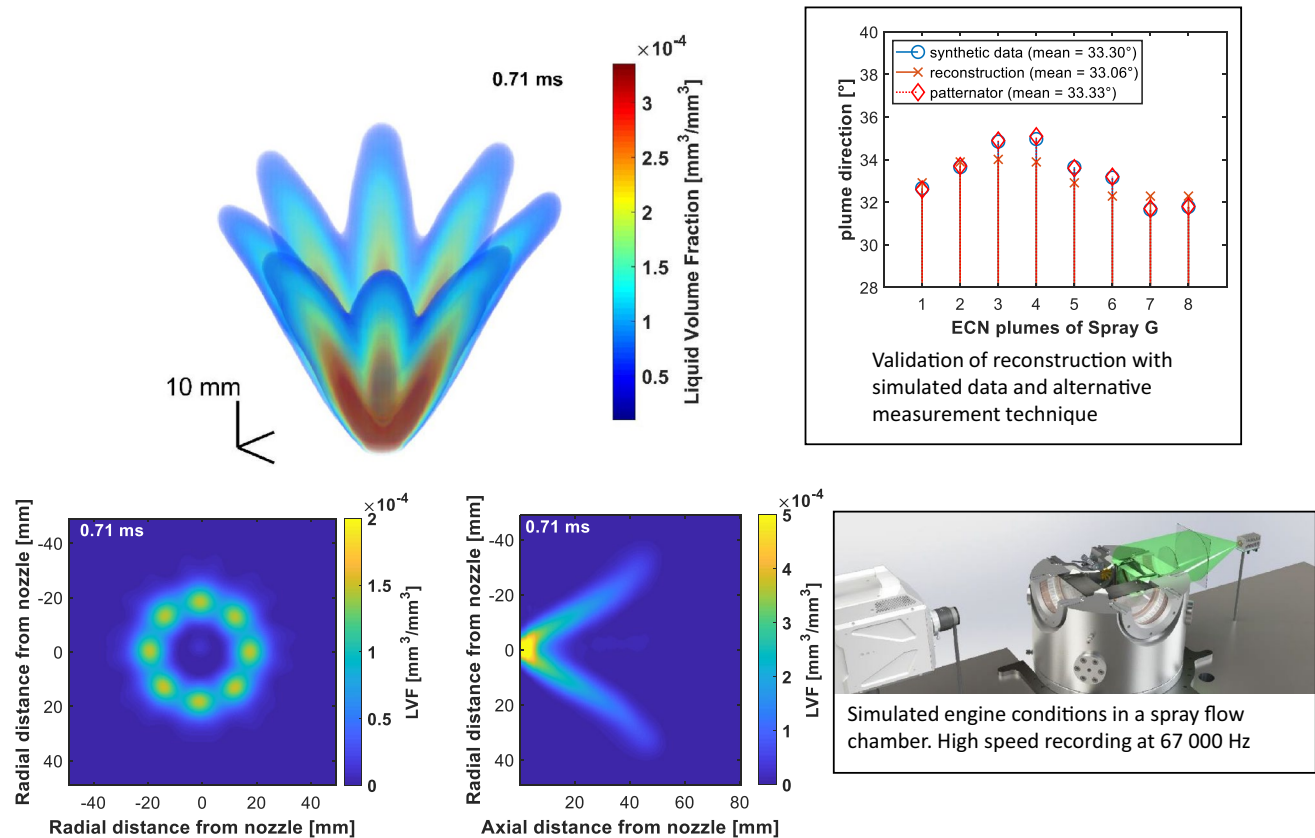
✉ Lukas Weiss
lukas.weiss@fau.de

¹ Institute of Engineering Thermodynamics, Friedrich-Alexander-Universität Erlangen-Nürnberg (FAU), Erlangen, Germany

² School of Advanced Optical Technologies, Friedrich-Alexander-Universität Erlangen-Nürnberg (FAU), Erlangen, Germany

³ Sandia National Laboratories, Livermore, CA, USA

Graphic abstract



1 Introduction

Fuel direct injection into the combustion chamber of automotive engines offers many advantages for fuel efficiency. The challenge is to inject the fuel into this small volume without forming liquid films on any walls, while simultaneously distributing the fuel vapor to utilize all available air. Wall wetting and low air entrainment would lead to increased soot particle formation (Zhao 2009; Kim and Park 2006; Peterson and Sick 2009; Spiegel and Spicher 2010). Thus, a main task in the engine development is the spray layout. A design difficulty is that the spray plumes of modern multi-hole injectors induce a flow field and, thus, interact with each other. Especially under flash-boiling conditions, the plume direction varies strongly from the designed hole or “drill” angle, with interacting plumes merging completely into a spray “collapse” (Bornschelegel et al. 2017; Heldmann et al. 2015; Payri et al. 2017). The degree of plume interaction and spray collapse depends on the ambient conditions and fuel properties, as well as the injector design itself. While many diagnostics have

been developed seeking to quantify gasoline direct injection (GDI) spray characteristics completely and quantitatively, from a practical perspective, identification of the plume direction, or essentially, “where the fuel goes”, is of utmost importance (Sphicas et al. 2017). Experiments designed to quickly characterize plume direction are useful for preparing CFD models for specific injection hardware. The CFD models offer the potential for design optimization for fuel delivery.

Experiments are, therefore, performed to measure spray characteristics. An industry standard is to use mechanical patternation at room-temperature and pressure conditions, as defined in the Society of Automotive Engineers (SAE) J2715 standard (SAE 2007). The technique to define plume orientation in J2715 is defined here for terminology familiarity and relevance for later discussion. An injector is mounted at a prescribed Vertical Test Distance (DTV) above and perpendicular to a grid with square or hexagonal collector cells. After a prescribed injection duration, the mass in each cell is weighed and the plume region mass-weighted centroid (DC) is calculated, relative to the

injector axis. The direction of the plume to the patternator position is defined as the Cone Bend Angle:

$$\text{SAE } J_{2715} \text{ Cone Bend Angle} = \tan^{-1} \left[\frac{\text{DC}}{\text{DTV}} \right], \quad (1)$$

Although useful for consistency and standardization, there are obviously many limitations to such patternator tests for characterizing an actual spray in an engine. Mechanical patternation is a time-integration of the spray footprint and will not reveal changes during injection. As it is collected liquid fuel mass, vaporized fractions are ignored. Based upon a single axial position, it does not reflect any bend in the plume during time or space. Perhaps most importantly, the measurement is performed at temperatures and pressures far from that in an engine.

To guide CFD, it is important to have a detailed understanding of the spray mixture and plume direction under realistic engine conditions, both temporally and spatially resolved. Optically accessible spray chambers have been developed to mimic engine conditions, and different approaches have been applied to measure plume direction. These can be summarized as line-of-sight imaging, sheet imaging and non-imaging techniques.

State of the art line-of-sight measurements are shadowgraphic or scattering methods, providing time-resolved measurement of spray vapor and liquid envelope (Parrish 2014). Injector rotation to produce different plume orientation permits measurement of different envelope along the line of sight, but provides less information about individual plumes, especially those overlapping along the line of sight. However, some analysis is possible. For example, Sphicas et al. (2017) applied extinction imaging of liquid plumes in a perspective that permitted identification of maximum extinction corresponding to the plume center. Using knowledge of the drill-hole positions and other geometry considerations, they then derived the plume direction relative to the injector axis, showing collapsing sprays with increasing ambient temperature or with longer injection duration (Sphicas et al. 2018).

Planar laser diagnostics could theoretically provide detailed information about plume direction at an illumination plane. However, in optically thick sprays, these methods suffer from multi-scattering effects and laser light attenuation, making quantification difficult. The Structured Laser Illumination Planar Imaging (SLIPI) method has been applied to correct for multiple scattering, but the light attenuation (obscuration) problem and signal-trapping problem remain (Berrocal et al. 2008). For example, SLIPI-corrected images in a GDI spray show massive differences in intensity on the “illumination” side compared to the “dark” side of the spray (Berrocal et al. 2008), thereby failing to provide a relationship between collected Mie-scatter signal and liquid volume fraction. A two-photon fluorescence method has also been

implemented to reduce multiple-scattering effects on planar imaging in a GDI spray (Berrocal et al. 2019), but attenuation of the incoming laser light and signal trapping remain important, and it is not clear that the technique could be applied at higher optical thicknesses. Similar concerns may be cited for a two-pulse SLIPI technique recently applied to a GDI spray (Storch et al. 2016).

Non-imaging optical techniques such as laser Doppler velocimetry (LDV) and phase Doppler interferometry (PDI) are also applied to understand plume direction and spray characteristics. PDI offers local measurement of droplet velocity and size at a focused crossing of two beams. By translating the probe volume through the plume, the plume center may be determined. For example, the plume center at a given axial position was defined as the position with highest droplet velocity magnitude for the Engine Combustion Network Spray G injector (Duke et al. 2017). Because the nominal injector and operating conditions (Spray G) were identical, the plume center determined by PDI could be compared to that derived from extinction imaging (e.g., Sphicas et al. 2017). Results showed a consistent decrease in plume direction (towards spray collapse) with time after the start of injection for two injectors with the same Spray G specification (Duke et al. 2017).

X-ray extinction radiography along a line-of-sight does not suffer from multiple-scattering and optical density concerns that are problematic for light imaging, particularly very near the nozzle. By performing X-ray extinction measurements from multiple perspectives and ensemble averaging using many injections, computed tomography may be applied to yield the local fuel mass per volume along a plane (Duke et al. 2015; Bieberle et al. 2009). Duke et al. scanned Spray G in three planes close to the injector tip (2, 5, 10 mm downstream), while rotating the injector 180°, at tight increments (e.g. 1°). Although the chamber for X-ray experiments could not be heated to the Spray G ambient gas condition (it was 300 K, rather than 573 K), the Spray G density was set at the correct 3.5 kg/m³ target. The plume growth and direction derived from fuel density fields measured by X-ray tomography were compared to that of the PDI and extinction imaging (Duke et al. 2017). The X-ray tomography showed that the plume direction angles are less than the measured geometric-hole drill angle (36°–38°), indicating already-deflected internal-nozzle flow that could affect plume interaction downstream. Although the X-ray measurement technique provides tomographic data in a non-accessible dense spray area for visible light measurements, it suffers from restricted ambient conditions and lack of access to most industrial researchers.

Optical extinction measurements from multiple perspectives, coupled to computed tomography to reconstruct local features, have shown promise in some applications. A limited-view tomography approach was recently performed

by Klinner and Willert (2012). Four double-shutter cameras were placed in 30° steps around the spray and were simultaneously triggered/synchronized to inexpensive LED short-pulse lighting. The three-dimensional distribution of droplets, and the ring shape of the hollow cone spray were reproduced quite well at obscuration (attenuation) levels where holography would not work (Klinner and Willert 2012). These results suggest that optical extinction from multiple views and computed tomography may overcome multiple-scattering and obscuration limitations associated with laser-sheet scattering or fluorescence.

Commercial optical extinction tomography systems are available, serving a role as spray patternator but without some of the mechanical patternator constraints. For example, an instrument using laser sheets and detectors from multiple views provides tomography data on a plane with 10-kHz temporal resolution, but in an unenclosed, room-condition spray (“En’Urga Inc.” and “SETscan OP-400 brochure” 2019). The system is similar to the earlier work from McMackin et al. (1999). Line-of-sight units along a plane are also available, and have been applied to windowed spray chambers at engine-relevant pressures and temperatures including intake-injection as well as late-injection conditions (“En’Urga Inc.” and “SETscan OP-400 brochure” 2019; Parrish et al. 2010). To facilitate tomography for planar data, the injector was rotated in 22.5° increments in a total of eight views to cover full 180° rotation. Data were acquired at 1 kHz at each view, and an average of 25 injections was processed for the reconstruction. The dataset identifies major changes in plume position and growth with variation in chamber conditions (Parrish et al. 2010).

In this work, we extend the optical extinction tomography on a plane at 1 kHz to full imaging extinction tomography

at 67 kHz, performed in a controlled chamber using an ECN Spray G injector. The result is a three-dimensional liquid volume fraction dataset that provides unprecedented ability to track individual plumes in space and time for a multi-hole GDI injector under engine-relevant conditions. Our approach is to use the characteristics of a symmetric 8-hole injector to discover the number of limited views required to efficiently characterize the mean behavior, rather than to apply full detailed tomography. To guide the experiment, we first use modeled (synthetic) spray data to understand compromises associated with the limited views, assumptions, and tomographic reconstruction to recover the original synthetic data. We then apply the diagnostic at target ECN spray chamber conditions, comparing results against previous observations of Spray G.

2 Tomographic reconstruction of synthetic data

To develop the limited-view tomographic reconstruction method, we use a synthetic model dataset where the “answer” for three-dimensional liquid volume fraction is known, allowing a test of the tomographic reconstruction methodology. The procedure is presented in Fig. 1. The one-dimensional control-volume jet model by Musculus–Kattke (2019) is used to generate liquid volume fraction (LVF) data for a single plume of the ECN Spray G injector (Musculus and Kattke 2010; Engine Combustion Network 2019). Inputs for this model are the measured spray cone angle, the mass flow rate, the hole dimensions, fuel properties and ambient properties. We then assemble all 8 plumes to represent a modeled spray where each plume is inclined using the

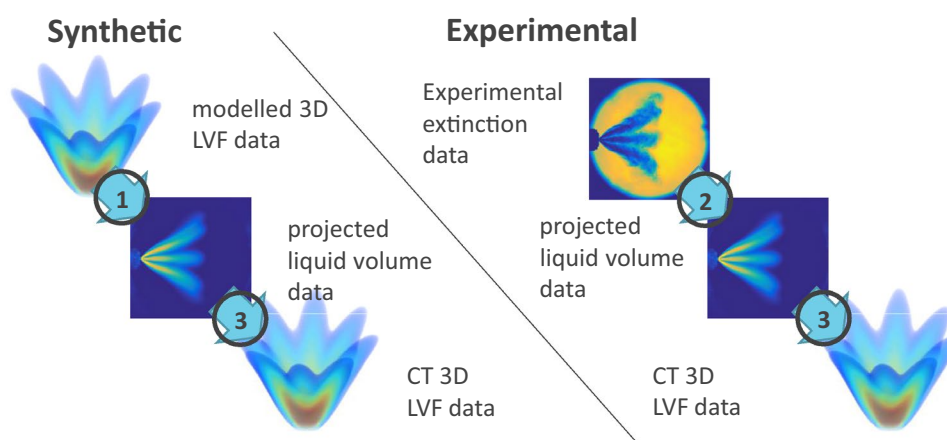


Fig. 1 Schematic pathway of synthetic and experimental data processing. The synthetic 3D LVF data are derived from the Musculus–Kattke model (Musculus and Kattke 2019). In step 1, these data are integrated along one spatial axis to generate synthetic projected liquid volume (pLV) data, which is comparable to the experimental pro-

jected volume data. The experimental pLV is transformed via Mie-theory from extinction measurements in step 2. The pLV computer tomography (CT) processing (step 3) is identical for the synthetic and the experimental pLV data. This method allows to qualify the limited-view CT results with the known original synthetic LVF data

measured Cone Bend Angle (see Eq. 1) from mechanical patternator data, which incorporates variances in direction for each plume for Injector #28 (Manin et al. 2015). These data were taken by Delphi, the donators of ECN Spray G, using a DTV of 50 mm, room-temperature, n-heptane fuel, and a 1.5-ms injection at 20-MPa pressure (Manin et al. 2015). The resulting “footprint” at an axial plane of 15 mm is shown in Fig. 2 in the top left corner. Later, we will compare plume direction results obtained from this synthetic input data against CT reconstructed synthetic data.

At this point, we want to highlight that measuring a plume direction from a “footprint” or centroid at a particular axial plane can create a bias in the measurement, a fact also acknowledged in SAE J2715 standard (SAE 2007). The plume axis is indicated as the dashed line in Fig. 2. In fact, it is the trajectory of the plume center and is not necessarily a straight line. But for the plume direction measurements, it is considered as a straight line from the plume center to the origin of the drill hole, which is also considered to be the origin of the plume itself. A common way to determine the plume center is to apply the full width at half maximum (FWHM) method on the footprint data. Basically, the edges

of the spray plume at a certain threshold are detected and the center is assumed to be in the middle of the edges. Figure 4 shows the centerline plot of a plume footprint and the corresponding FWHM threshold. If the measurement plane is inclined with respect to the plume axis normal, the footprint in the measurement plane would be compressed towards the injector axis and elongated on the opposite side when using a FWHM definition, as depicted in Fig. 2 at the green cross. The results off the FWHM method are shown in Fig. 4 where the vertical dashed black line indicates the FWHM plume center and the red line the actual plume center. Different concerns and biases arise when using mechanical patternator centroid data, which is affected by integrated mass flux to the plane. The footprint corresponding to a plume direction is even more challenging if the plume axis is not on a straight line, but bended due to plume-to-plume interaction (Duke et al. 2015). Thus, the specific definition for plume direction angle needs consideration when comparing results to other studies, as well as to CFD predictions. In this study, the plume center is defined by the peak value of LVF in the footprint at a certain axial plane, which corresponds to the crossing of all three-colored lines in Fig. 2, and is free of any

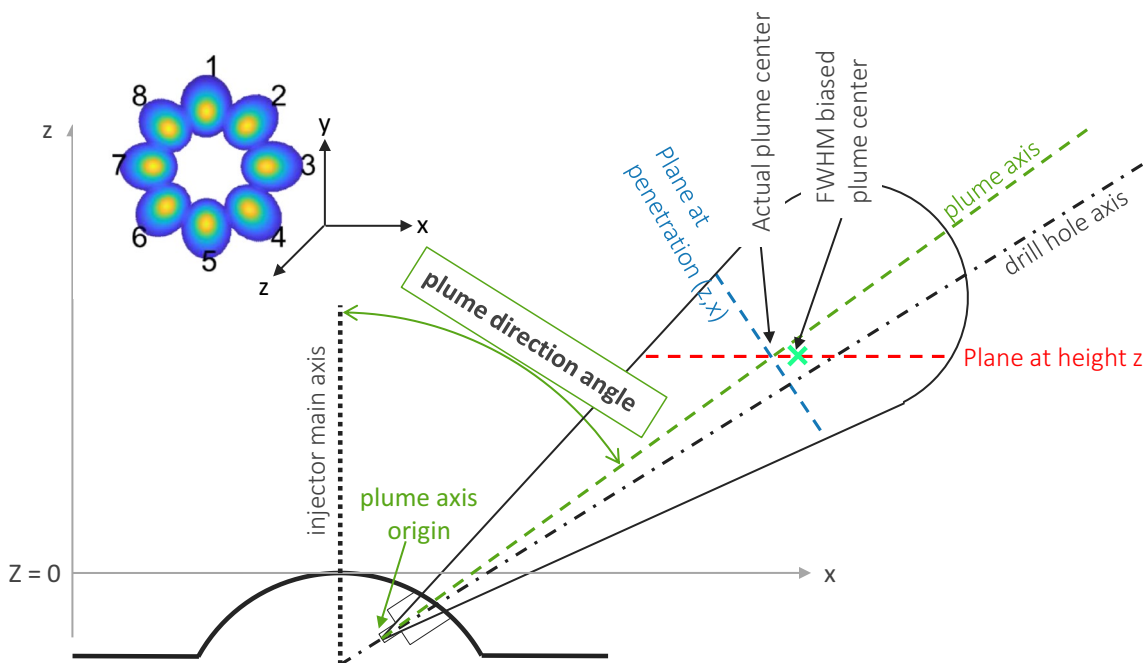


Fig. 2 This schematic defines the correct plume center and plume direction angle and illustrates possible biases. The plume direction at a specific height z is the angle between the injector main axis and the plume axis. The plume axis is defined by two points: (1) the origin of the plume axis which is the same like the drill-hole origin; (2) The location x of the maximum liquid volume fraction in the measurement plane z . This point cannot be found by a FWHM approach, because the plane at height z is not perpendicular to the plume axis. Thus, a FWHM approach would create a bias towards the outside of

the spray indicated by the green cross. To demonstrate that a X - Y slice of the synthetic spray data is presented in the top left corner showing the ECN plume footprint and numbering at an axial plane of 15 mm looking towards the injector. The steeper gradient towards the center of the LVF compared to the outside is the reason for the bias. Another type of bias in the definition of the plume direction angle is due to the selection of the nozzle tip instead to the plume origin as a second point of reference

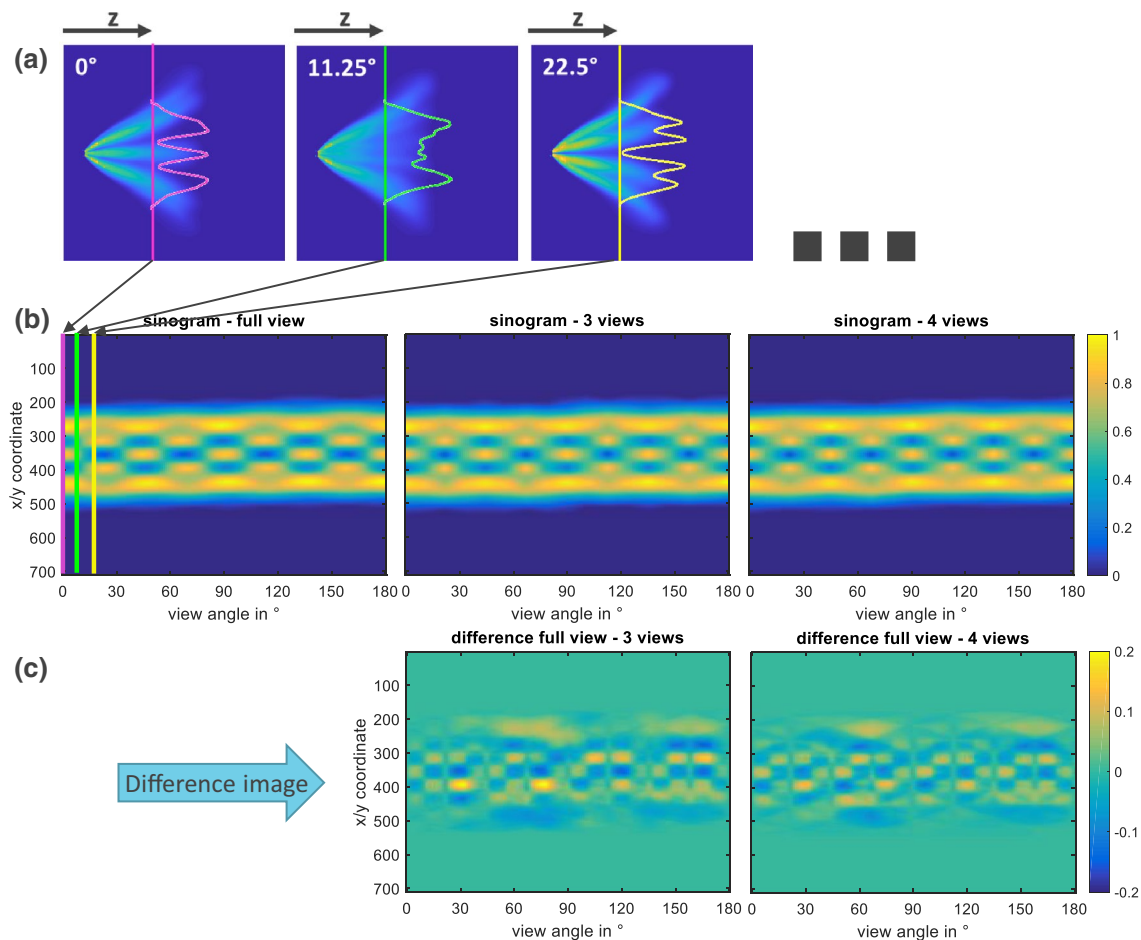


Fig. 3 **a** Line intensities of pLV data at a certain z position is stacked together to a sinogram. **b** Sinogram of the full and the limited-view variants are presented. The limited-view sinograms are continuous

and only differ slightly from the full view. **c** Subtracted images are displayed to highlight the differences from the full view

bias (unlike a FWHM definition). This bias is also illustrated by the dashed lines in Fig. 4. Another type of bias to be avoided besides the FWHM stems from the assumption that the plume origin is at the nozzle tip and not in the drill-hole origin, like in the SAE J2715 standard, which creates a relevant error evaluating plume directions close to the injector.

Step 1 in Fig. 1 is a simple line integral along different radial vectors of the 3D LVF data to represent the experimental process to measure optical thickness along a line of sight with different injector rotations. So, the three-dimensional data are projected on equivalent x - y plane. Repeating these projections at certain rotational view angles from 0° to 180° provides synthetic planar projected liquid volume data for the tomographic reconstruction, which is equivalent to the experimental projected liquid volume data. In contrast to the synthetic data, the experimental data are derived in step 2 of Fig. 1 from extinction measurements. The transformation from extinction measurements to projected liquid volume data is described later in the experimental section

of this paper. In step 1, the chosen step size for the rotational view angles was 1.125° for the “full-view” reconstruction. The algorithm processes each z -plane independently. When extracting one z -plane from each image, the lines can be stacked and plotted as a sinogram to check continuity in the data. After some evaluation, a limited 3-view setup with view angles 0° , 22.5° (equivalent to ECN primary and secondary view) and 11.25° was selected. For the limited 4-view version, view angles 0° , 22.5° and their 90° complementary views 90° and 112.5° were chosen. Since Spray G has a symmetric 8-hole configuration, the image of the spray is expected to be quite similar every 45° . This assumption was used to fill data into the sinogram at every 45° of the base views. The gaps between were linearly interpolated. The resulting sinograms are continuous, but differ slightly from the original, Fig. 3b, c. Sinograms are the input data for the inverse Radon function (Bieberle et al. 2009; Kak et al. 2002). A sinogram is actually a stack of line integrations of a certain plane of the 3D data set along different rotational

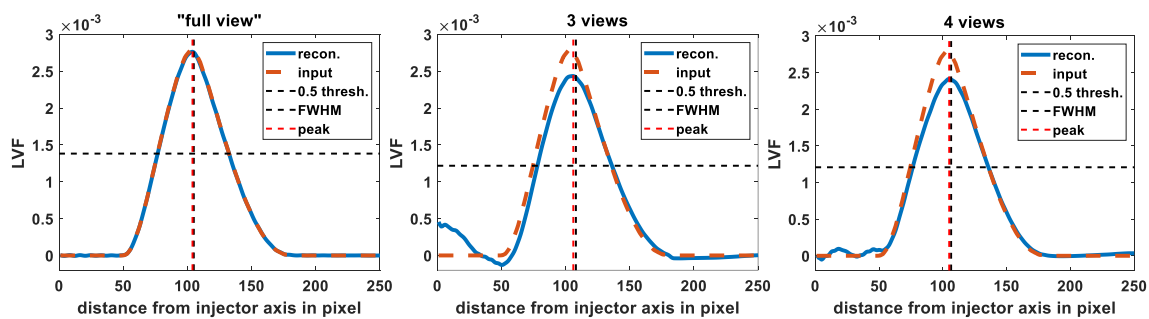


Fig. 4 The full-view reconstruction reproduces the line data of the LVF in a certain z -plane from the spray center to the edge with low deviation. Only the peak value is slightly decreased to 96%. The limited 3-view reconstruction show a distorted peak area and artifacts up

view angles from 0° to 180° . This is exemplarily shown in Fig. 3a. Whereas in the “full-view” a planar data set for each angle is available, the missing angles for the limited views are filled by linear interpolation. The built-in MATLAB iradon function, which uses the filtered back projection algorithm to perform the inverse Radon transform (Kak et al. 2002), is used to tomographically reconstruct the data for both detailed and interpolated limited-view applications. A Hamming filter of 0.6 is applied for the algorithm. The filter setting has no significant effect on plume direction measurements, but a higher value is favorable to reproduce the peak value better. To evaluate the quality of the reconstruction, the LVF is plotted along a line cutting through the plume center from the injector axis as shown in Fig. 4. The peaks in these curves define the plume center, as mentioned before. The “full-view” reconstruction shows very tight replication of the input line profile, as calculated by the Musculus–Kattke model, with the peak value decreased to 96% of the original. The limited-view reconstructions drop further to 85% (3-views) and 87% (4-views), but retain the same peak location. However, the 3-view result shows artifacts in the center region, reaching almost 20% of the signal intensity. The artifact remains but is significantly decreased in the 4-view version.

Although we used the mechanical patternation results from Delphi as input for our synthetic data, an offset of 0.03° occurs because of data manipulation, but this is of no consequence. The nearly identical patternator and synthetic plume direction angles are plotted as reference in every subplot of Fig. 5. The tomographic reconstruction algorithm reproduces the synthetic data angles within 0.02° , when using 160 views (1.125° stepping, “full-view”) as shown in the top left subplot. When limiting the views to only three, the average plume direction is still within 0.25° . Some plumes have more offset than others, but even the general trend is correct. Adding one more view (to four) improves the overall agreement for the average and individual plume direction angle but does not eliminate the scatter.

to 20%. Only one additional view reduces the artifact significantly. The actual peak position and the FWHM peak position are indicated by dashed lines showing the biases of an inclined measurement plane

In a line of sight perspective, plumes that are overlapping (and their variances) may be harder to identify in a reconstruction, than ones in the periphery of the spray that stand out alone. For example, having a camera set from left to right referring to the spray footprint in Fig. 2, plumes #7 and #3 would be seen as one plume; while plumes #1 and #5 are outstanding. Thus, we rotated the input data 90° to change the major line of sight perspective to determine how the reconstruction is affected for limited-view situations (bottom of Fig. 5). The resulting individual plume directions are different, but the averages are not significantly influenced. There is no evidence that plumes #7 and #3 are reconstructed worse than #1 and #5 before rotating and better after rotating the input files. It is rather that the overall representation is slightly worse in the bottom row.

Figure 6 shows the results of a hypothetical injector with a single extraordinary spark plug plume at 42° , while all other plumes have a direction angle of 37° . The unlimited reconstruction can perfectly represent the plume directions of every single plume, while the limited 3-view approach cannot resolve the single extraordinary plumes. The 4-view reconstruction rises in the correct direction for the extraordinary plume, but is still about 3° – 6° off.

The synthetic data study shows that the used plume direction angle definition is a robust method. Using 160 views covering the full 180° results in an accuracy of 0.03° in plume direction angle. The limited 3-view approach reproduces the average plume direction with an error of less than 0.25° for a Spray G-like injector and, thus, is a suitable method to investigate ambient and fuel influences on spray targeting for this specific style of injector. The study shows that LVF peak values are underestimated, with an error range of 15%, but this may be tolerable as plume direction is the primary goal rather than actual LVF. Clearly, more views (like 160) would always be preferred for more faithful reconstruction, but this carries certain experimental costs that may not justify the extra effort

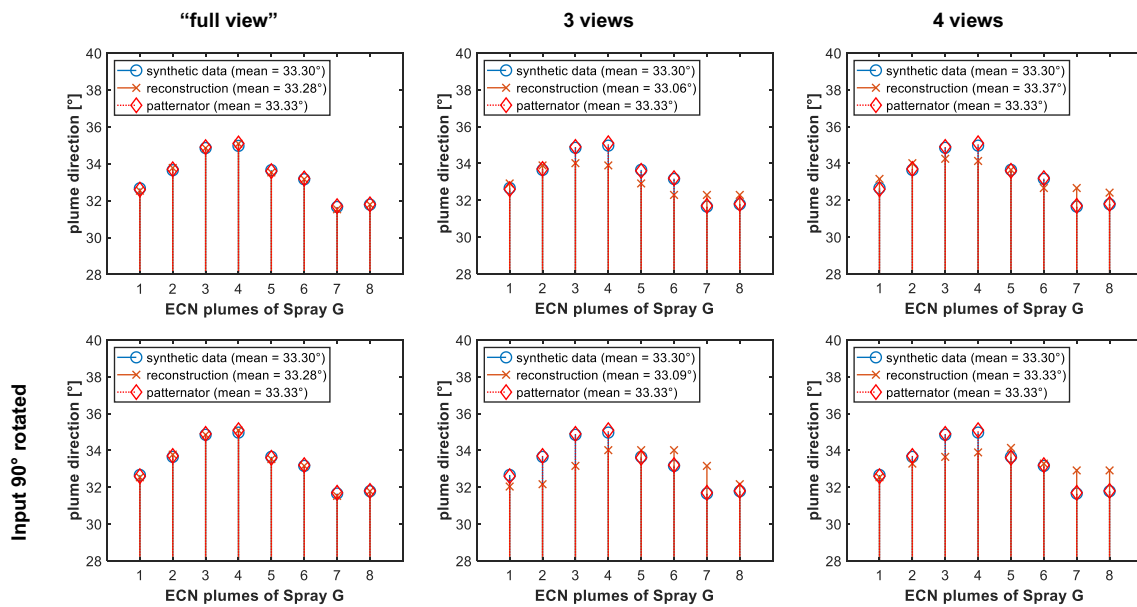


Fig. 5 Reproduction of the real plume directions (input from patternator data measured for Injector 28) applying the plume direction definition to synthetic and reconstructed data

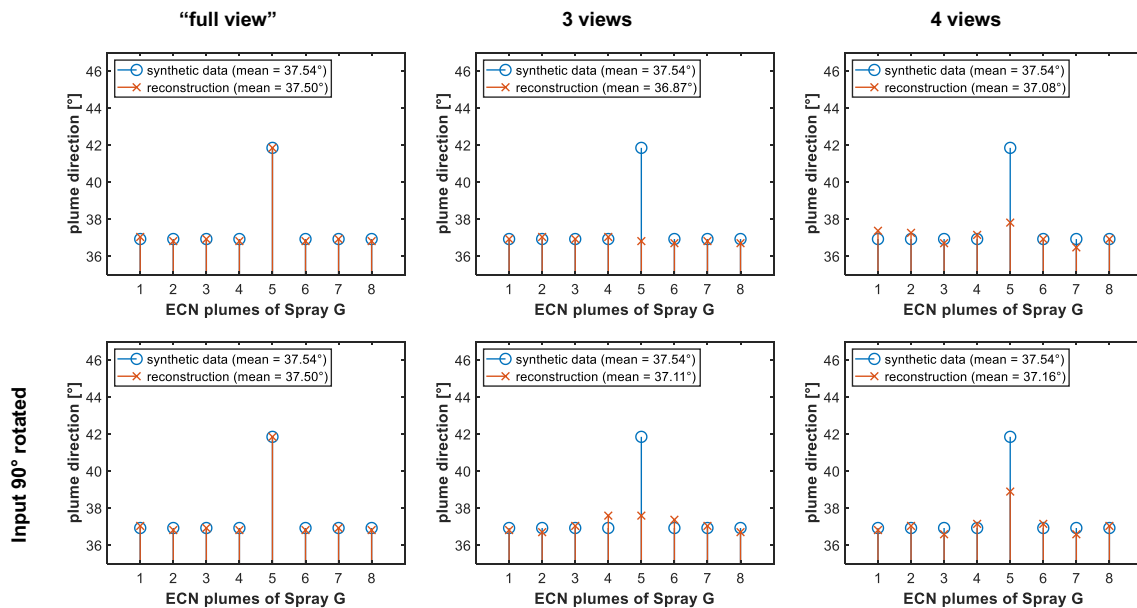


Fig. 6 Synthetic data analysis shows, that the method is not able to measure single extraordinary plumes, like a spark plug plume in side mounted GDi sprays

depending upon the injector. If different injectors are used, including those with asymmetric or extraordinary plumes, more views will be necessary. The synthetic data tool may be used to guide the setup for specific injectors.

3 Diffused backlight illumination extinction imaging (DBIEI)

The experimental input data for the tomographic reconstruction are derived from diffused backlight illumination extinction imaging (DBIEI) measurements. This diffuse illumination ensures that the intensity changes in the

image are due to extinction. Vapor-phase beam-steering is suppressed once the proper diffusion angle is used in the optical setup. Engineered diffusers supply a homogeneous light field within a certain diffusion angle. The optical fundamentals for the setup are discussed in (Westlye et al. 2017). The Engine Combustion Network (ECN) recommends extinction techniques (that also account for beam-steering) for liquid penetration measurements, because it is found to be the more reproducible technique over different laboratories in comparison to Mie-scattering imaging and the experimental results may be more closely compared to CFD simulations (Pickett et al. 2015). Extinction diagnostics permit self-calibration to the initial intensity, while a Mie-scatter signal can include biases due to inhomogeneous illumination in test rigs with minor optical access. As will be shown below, processed optical extinction experimental data can be quantified as a projected liquid volume (pLV) in hope of a direct comparison to CFD using the same metric. The ECN has defined two criteria for the liquid spray border:

$$pLV = \int_{-y_\infty}^{y_\infty} LVF \cdot dy, \tag{2}$$

$$pLV = \int_{-y_\infty}^{y_\infty} LVF \cdot dy = 0.2 \cdot 10^{-3} \frac{\text{mm}^3 \text{ liquid}}{\text{mm}^2}$$

AND $2.0 \cdot 10^{-3} \frac{\text{mm}^3 \text{ liquid}}{\text{mm}^2}$.

The two thresholds for the liquid boarder address different sensitivities in models and experiments. The DBIEI measurements provide cumulative quantitative data of the optical thickness τ along the beam path. The Lambert–Beer law formulates the relation between initial intensity I_0 and the measured intensity I :

$$I/I_0 = e^{-\tau}. \tag{3}$$

Mie-theory further relates the measured optical thickness τ to the liquid volume fraction (LVF), see Eq. 4. Berrocal et al. (2007) found that multi-scattering has not to be considered at an optical thickness up to 2, which is about the relevant region of a fuel spray.

$$\tau = \int_{-y_\infty}^{y_\infty} C_{\text{ext}}^* \frac{LVF}{\pi d^3/6} dy. \tag{4}$$

Experimental Modeling

$$\tau \frac{\pi d^3/6}{C_{\text{ext}}^*} = \int_{-y_\infty}^{y_\infty} LVF \cdot dy. \tag{5}$$

Thus, the pLV is directly correlated with the droplet diameter d of the spray droplets and their extinction cross section C_{ext}^* , which is again a function of the droplet diameter, the incident wavelength λ , the refractive index n_{fuel} of the media and the detection collection angle of the optical setup. ECN recommends the MiePlot software to calculate C_{ext}^* .

The droplet size distributions in Spray G and G2 were measured in the ECN community, respectively, with phase Doppler interferometry (PDI) (Duke et al. 2017; ECN 2019). The PDI data and the derivation of the pLVF for liquid penetration measurements were published at the ECN6 workshop (Engine Combustion Network 2018). The data show that the SMD is about 7 μm during the injection event in the vicinity of the spray, where it is relevant to detect the spray border, Fig. 7. The vacancies in the PDI plots close to the nozzle are due to optical thick regions, where light attenuation blocks the measurement signal. These optically thick regions also effect the DBIEI measurements. At Spray G conditions bigger droplets > 15 μm were detected after 1.5 ms in the spray center. At G2 conditions, the big droplets were measured at the spray edges after 1.5 ms. These big droplets may be droplet coalescence after the end of injection at 0.8 ms.

4 Experimental setup

The experiments were carried out in a constant-flow spray chamber at Sandia National Laboratories, Fig. 9. The maximum design operating conditions for flowing scavenging gas are at 150 bar and 1100 K. The gas flows from bottom to top

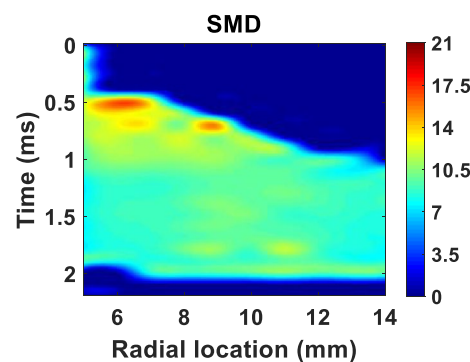


Fig. 7 PDI data of Spray G at G1 condition measured by Scott Parrish (GM) at $z=15$ mm for Plume 1 of Injector #16. The velocity data was published by Duke et al. (2017), the full data set is included in the primary Spray G dataset and published on the ECN website (2019). The data show that the SMD is relatively uniform at about 7 μm during the injection event in the vicinity of the spray, where it is relevant to detect the spray border

through a square cross section of 120 mm width, where the fuel is injected. After the heating coil, a diffuser is installed to homogenize the temperature and flow field. Gas temperature is monitored with three layers of eight thermocouples each: the first just above the diffused heater outlet, the second just below the measurement section and the third above the measurement section. Three pressure transducers with different range capability are installed in the chamber inlet. The stainless steel body is completely shielded with ceramic insulation in the inside. The chamber has one injector port and three optical windows of 125-mm diameter. The windows and chamber walls are actively cooled with water.

Experiments were performed at ECN Spray G2 and G3 conditions (Table 1), the solenoid ECN Spray G injector is independently temperature controlled to 90 °C with an additional water jacket. A thermocouple is pressed directly on the side of the injector tip to verify temperature. The injector has eight holes with counter bore and a drill angle of 37°; further injector specifications can be found on the ECN webpage, including 3-dimensional X-ray data of the hole shapes (Engine Combustion Network 2019). The specified

electronic duration provides an actual injection duration of approximately 0.78 ms.

The optical setup for DBIEI consists of a pulsed LED with a central wavelength of 519 nm. It is synchronized with the Photron SA-Z high-speed camera at 67,200 Hz. The image size is 512 × 512 pixels. The 80-ns LED light pulses from a custom driver are timed in the middle of the camera exposure. The LED light is collimated by a Fresnel lens ($f = 150$ mm, $d = 150$ mm) and then diffused by an engineered diffuser [diffusion angle 20°]. The diffuser is mounted onto the chamber window, to get as close as possible to the spray. The light passes through the chamber windows and the spray. A Nikkor 50 mm f/1.8 lens at aperture 2.8 is equipped with a 527 ± 22 nm bandpass filter. The distance from spray to the lens is $Q = 515$ mm. This setup resolves 0.19 mm per pixel. The collection angle is $\alpha = 69.3$ mrad according to Eq. 5, where the effective aperture of the lens A_{eff} is defined by the focal length f and the aperture A . Equation 5 can be simplified using the small angle approximation. The extinction cross section at this collection angle was calculated to $C_{\text{ext}}^* = 72.70 \cdot 10^{-6}$ mm², using the iso-octane refractive index of $n_{\text{fuel}} = 1.391$.

$$A_{\text{eff}} = \frac{f}{A}, \quad (6)$$

$$\alpha = 2 \cdot \tan^{-1} \left(\frac{A_{\text{eff}}}{2 \cdot Q} \right) \approx \frac{A_{\text{eff}}}{Q}. \quad (7)$$

For each injector position, 3 sets of 100 injections were recorded, individually processed to pLV data and then averaged. Exemplary raw images from each view are shown in Fig. 8. 400 frames per injection cover a time span of about 6 ms including data during and after injection. Before each set, 400 background (dark) frames were recorded with no lighting, and the initial intensity was measured for 15 frames

Table 1 ECN operating conditions (Engine Combustion Network 2019)

Parameter	G2 flash-boiling	G3 early injection
Fuel	Iso-octane	Iso-octane
Fuel temperature	90 °C	90 °C
Ambient temperature	60 °C	60 °C
Fuel pressure	20 MPa	20 MPa
Ambient density	0.5 kg/m ³	1.12 kg/m ³
Ambient pressure (using nitrogen)	(50 kPa)	(100 kPa)
Electronic injection	0.680 ms	0.680 ms
Injected mass	10 mg	10 mg

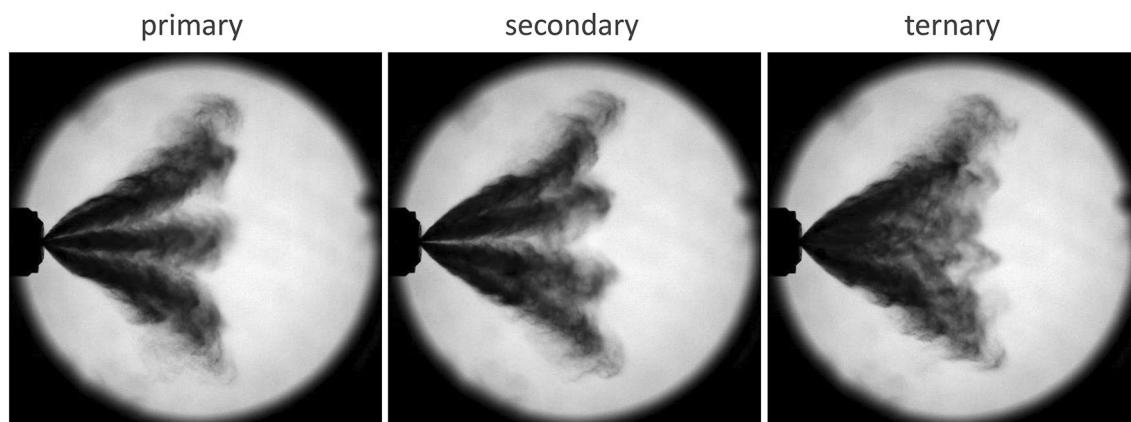


Fig. 8 Example raw images of the extinction measurement. Operation point G2 at 0.7 ms after visual start of injection

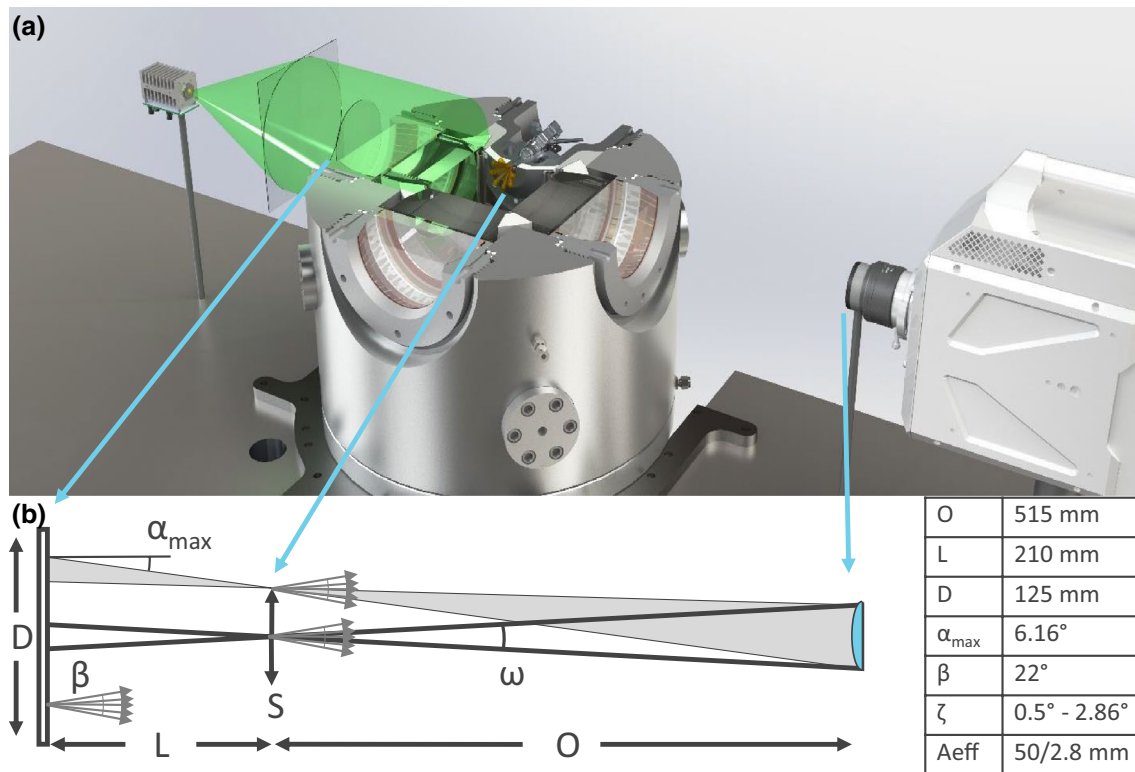


Fig. 9 **a** Cut-through of the constant-flow spray chamber at Sandia National Laboratories showing the optical DBIEI setup. **b** Sketch and data to calculate the schlieren-free image zone of a given DBIEI setup according to (Westlye et al. 2017)

prior to injection to understand the mean I_0 pixel by pixel (Fig. 9).

Importantly, the background and I_0 are completely within the count range of the camera (no zero or saturated pixels), making it possible to accurately measure I . Also, we considered linearity effects of the camera at the bottom and the top of the sensitivity range. The injector was rotated anticlockwise, when looking at the nozzle tip, to three different views: the ECN primary view (0°, view 1), the 11.25° angle (view 2) and the ECN secondary view (view 3) at 22.5°. The mechanical rotation indicator is placed about 150 mm off axis to allow precise angle alignment. The rotation was performed by rotating the whole injector mount.

5 Data processing

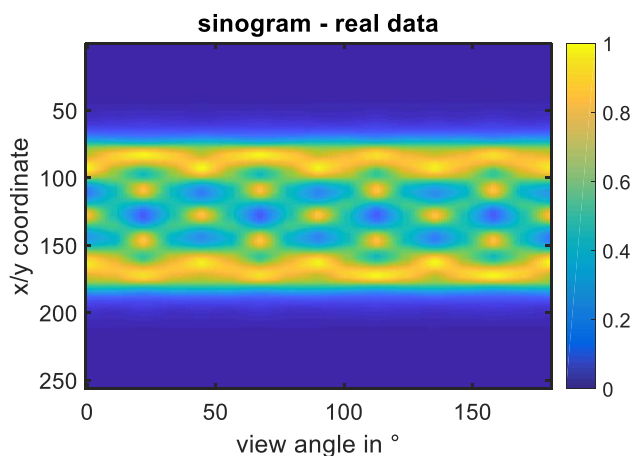
The data sets for each view were translated to projected liquid volume fraction data individually. In a first step, all images of one timestep were background subtracted. Next, a dynamic I_0 correction was performed. For that purpose, two areas of 10×10 pixels each that remain outside of the spray region for the entire injection were selected. The average intensity value of each image was compared to a reference image and consequently a correction factor was applied.

These averaged and corrected intensity values were then translated into pLV values using Eqs. 3 and 5. Before the tomographic reconstruction, the data were then averaged. It is important to average after transforming into pLV to avoid biases up to 10% for optical thicknesses of 2 (Musculus and Pickett 2005).

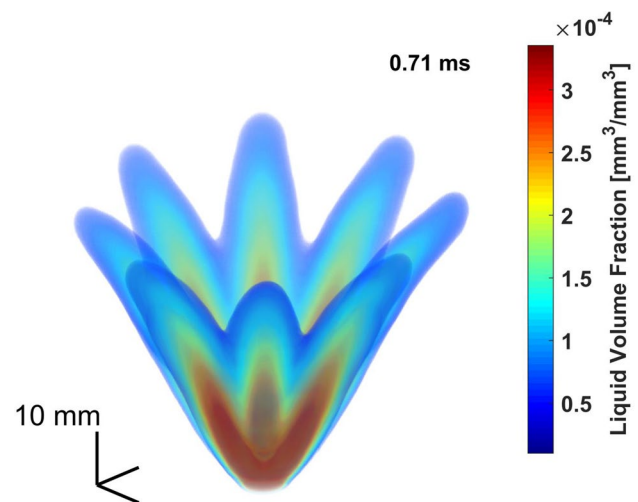
For tomographic reconstruction, the individual view data at each rotation are processed using parallel graphics processing unit (gpu), because each z -plane is reconstructed individually. The sinogram is built using the algorithm illustrated in Table 2, which is exactly the same algorithm used for reconstruction of the synthetic model data as demonstrated in the limited 3-view results given in Fig. 5. Table 2 shows that the measured data are flipped (inverted) and combined to provide the proper input to the sinogram if the injector had been rotated to that position. For example, the 180° input is the flipped of View 1 at 0°. Sinogram inputs for other intermediate angles exercise the assumption of symmetry, justified because of the symmetric design for this particular injector. By adding additional views, we provide that specific information to the algorithm. This is the key step to transform the limited data to a “full-view”-like dataset. The inputs also enforce continuity at intermediate angles by combination of different views. The missing angles are filled with the *iradon*

Table 2 Construction of 0° – 180° of the sinogram using the symmetry information of ECN Spray G

3-view assemble		4-view assemble	
0°	view1	0°	view1
11.25°	view2	11.25°	$(0^\circ + 22.5^\circ)/2$
22.5°	view3	22.5°	view2
33.75°	view2	33.75°	$(22.5^\circ + 45^\circ)/2$
45°	$(\text{view1} * 3/4) + (\text{flip}\{\text{view1}\} * 1/4)$	45°	$(\text{view1} + \text{view3})/2$
56.25°	view2	56.25°	$(45^\circ + 67.5^\circ)/2$
67.5°	view3	67.5°	flip{view4}
78.75°	view2	78.75°	$(67.5^\circ + 90^\circ)/2$
90°	$(\text{view1} * 2/4) + (\text{flip}\{\text{view1}\} * 2/4)$	90°	view3
101.25°	flip{view2}	101.25°	$(90^\circ + 112.5^\circ)/2$
112.5°	flip{view3}	112.5°	view4
123.75°	flip{view2}	123.75°	$(112.5^\circ + 135^\circ)/2$
135°	flip $\{(\text{view1} * 3/4) + (\text{flip}\{\text{view1}\} * 1/4)\}$	135°	$(\text{flip}\{\text{view1}\} + \text{view3})/2$
146.25°	flip{view2}	146.25°	$(135^\circ + 157.5^\circ)/2$
157.5°	flip{view3}	157.5°	flip{view2}
168.75°	flip{view2}	168.75°	$(157.5^\circ + 180^\circ)/2$
180°	flip{view1}	180°	flip{view1}

**Fig. 10** Sinogram assembled from 3 views of real experimental data from G2 iso-octane at 0.7-ms and 30-mm nozzle distance

spline interpolation method. The final sinogram is shown in Fig. 10 as continuous and smooth and looks similar to the synthetic data in Fig. 3. The use of only three views cannot be recognized, while the rotational symmetry in the sinogram is obvious. The tomographic solution from the sinogram is solved using the Matlab *iradon* function. Recall from Fig. 5 that this 3-view algorithm is capable of detecting some asymmetry between plumes, despite the simplifying assumptions, with a mean plume direction error of less than 0.5° .

**Fig. 11** 3D reconstruction of the G2 iso-octane spray. A threshold is applied to unveil the shape of the spray. Transparency allows to see inner LVF iso-surfaces as well. The outer box dimensions of the spray are about $80 \text{ mm} \times 80 \text{ mm} \times 60 \text{ mm}$. The movie is accessible on the ECN website: <https://ecn.sandia.gov/data/SprayG-Tomography>

6 Experimental results

The three-dimensional LVF distribution at a specific time for the G2 condition is shown in Fig. 11. A threshold is applied to show an iso-surface of LVF. The iso-surfaces are translucent to reveal regions of higher concentrations inside the spray as well. The axes are not displayed, but the outer box of the displayed spray is about $80 \text{ mm} \times 80 \text{ mm} \times 60 \text{ mm}$. The full data set has

$512 \times 512 \times 512$ pixels in space at a resolution of 0.19 mm/pixel. The temporal resolution is 0.015 ms/step and covers 6 ms. The resulting 3D data file has a size of ~ 30 Gb. To decrease data size, the spatial resolution of the projected liquid volume data can be divided by two without impact of plume direction measurements in downstream regions > 30 mm. However, the images in this work show full resolution results. The high resolution has benefits in the near nozzle area < 10 mm. As mentioned previously, the measurement is not designed to resolve the optically thick zones immediately at the nozzle exit.

Any slice of the data set can be selected, displayed and analyzed, as shown in Fig. 12. This is a huge advantage amongst other imaging techniques, where only one plane or line of sight data is available. Figure 12a shows a cross section normal to the central axis 30 mm downstream just before the end of injection at 0.7 ms. The single plume centers are clearly visible. Figure 12b shows a cross section through the injector main axis. Close to the nozzle exit, the LVF is very high and the spray plumes are not separated simply because of insufficient measurement resolution. As mentioned previously, we choose to do no analysis in this region. Distinct plumes are identified at 5 mm. Downstream, the plume head is bent outwards towards larger radii than the rest of the upstream plume, but there is no direct line in the plume back to the hole origin. The time sequence shows that the plume head is less influenced by plume-to-plume interaction because the flow field is not developed yet (Heldmann et al. 2015).

We can now process the dataset for plume direction, and apply the same methods and definitions developed for the synthetic model data where the actual plume direction is known as an input from the mechanical patterning data. While it is easy to select the corresponding measurement

plane at 50 mm, it is not clear which time of the temporally resolved optical data should be chosen for a suitable comparison. Therefore, Fig. 13 show results at different axial positions and timings, where the plume direction is a line back to the injector similar to the SAE J2715 standard given by Eq. 1.

No matter the condition, timing, or position, the average plume direction angle decreases during time. Slightly before end of injection (0.8 ms aSoI), the spray head passes the 50-mm plane, suggesting that there is no sustained period of steady behavior at any axial position. After the end of injection, the spray stretches from the nozzle and moves further downstream. The shape of the spray remains and slowly vanishes, but the tendency is for the plume direction angles to decrease over time (i.e., for the plumes to move together). When the spray root passes a measurement plane, single plumes may not be detected because there is no significant peak in the LVF anymore. For example, see the 15 mm data in Fig. 13c at 1 ms.

Using the data at G2 and G3 conditions at 1 ms, the measured plume directions for all plumes are plotted together with the mechanical patterning data in Fig. 13d. As expected, the G2 plume direction angles are lower than in the G3 cases, due to higher plume-to-plume interactions at flash-boiling conditions. The average plume direction angle deviates from the patterner for $+0.5^\circ$ at G3 conditions and for -2° at G2 conditions. In any case, the measured plume direction angles are considerably lower than the drill-hole angle, which is 37° indicating strong plume-to-plume interaction even at ambient and G3 conditions. The optical measurements confirm the trend of the single plume directions. Plumes #3 and #4 have the biggest direction angle, while #7 and #8 have the lowest.

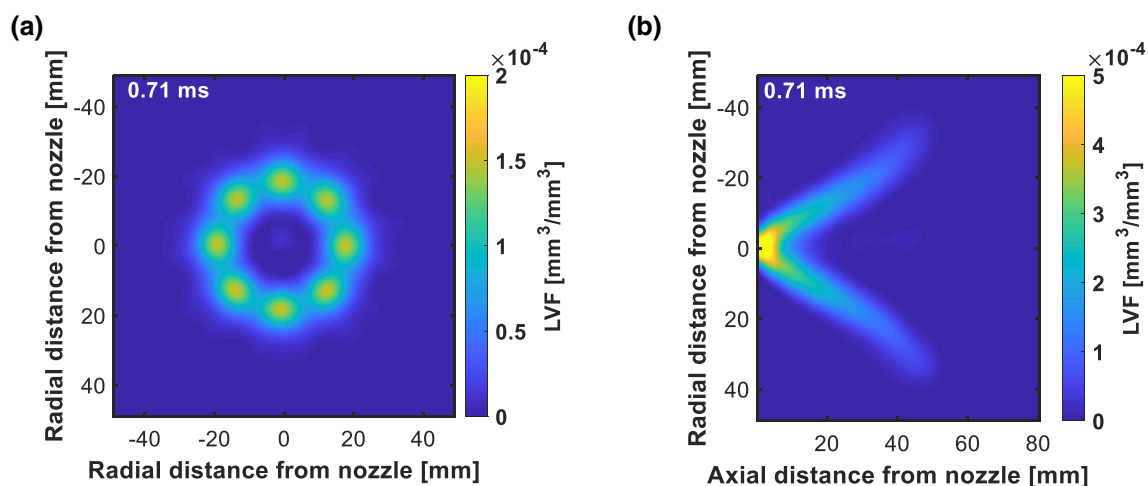


Fig. 12 Slices through the 3D data at conditions of Fig. 11 unveils inner structure of the spray and allows plume direction analysis: **a** XY-slice at 30-mm distance from the nozzle. **b** ZY-slice through the

spray center. CAUTION: different colorbar in (a) and (b). The movies are accessible on the ECN website: <https://ecn.sandia.gov/data/Spray-G-Tomography/>

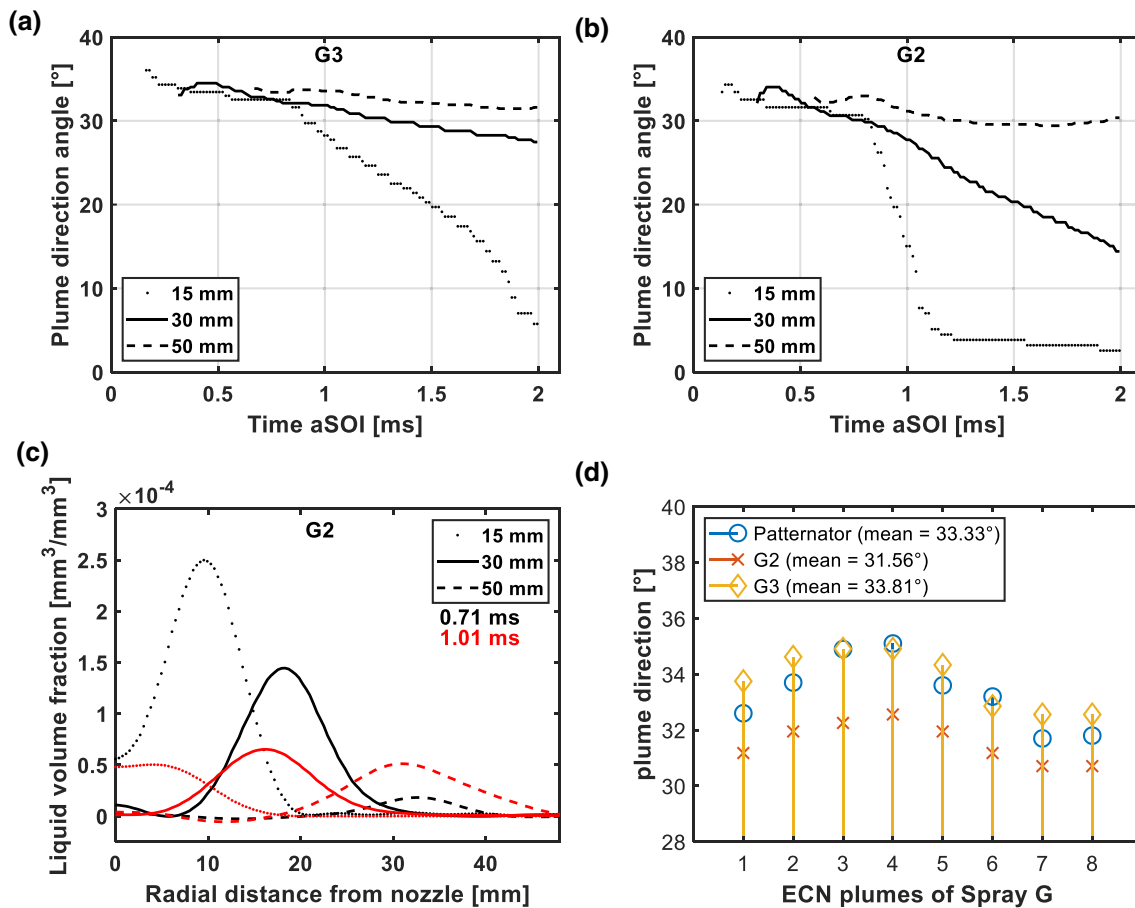


Fig. 13 **a** Average plume direction decreases over time at G3 conditions, measured at 3 different distances from the nozzle. **b** corresponding plot of average plume direction versus time for G2. **c** LVF centerline shows plume centers during and after injection at different locations. In any case the center peak is significant. **d** Comparison of

patternator data against optically measured plume direction at corresponding 50 mm nozzle distance and 1 ms avSOI. G3 has less plume-to-plume interaction, thus very close to the patternator data, while G2 plume directions are bend inwards for about 2°

7 Mitigating uncertainty discussion

As stated in the Introduction, the major purpose of the limited-view tomography was to describe “where the fuel goes”, including the plume direction dynamics. However, we also wish to make LVF measurements that are as accurate as possible. In addition, there are some special concerns about extinction imaging within a chamber that can affect accuracy. We will discuss issues affecting measurement uncertainty in this section.

Although based upon direct measurements for this injector (Fig. 7), a major uncertainty associated with the absolute values of LVF is droplet diameter. Figure 14 shows that absolute values of LVF vary depending on which droplet size is assumed, according to Mie scatter/extinction relationships. The range of droplet size chosen includes not only the main SMD measured during injection, but also larger droplets formed during ramp-down at the end of injection, and smaller droplets that must ultimately form as droplets

vaporize. For better quantification, one would need to have droplet size distributions for all positions and timings, which is an unfortunate limitation of more accessible optical techniques. Fortunately, the droplet size uncertainty does not influence the peak positions and the plume direction. We also accounted for the simplification from a multi-dispersed spray to a mono-dispersed one. An inhomogeneous cloud of droplets with a certain droplet size distribution and an SMD of 7 μm may not necessarily have the same optical properties like a monodispersed cloud of droplets with the same SMD of 7 μm . But other studies only mention a weak dependency of the scattering phase function on drop size variance for poly-disperse sprays (Lim et al. 2018). Thus, this uncertainty is subject for further investigations in scattering-based quantification and tomography.

Other uncertainties are created by the nature of optical access to the spray chamber. The high-speed extinction imaging method is easily applicable to any spray vessel or combustion chamber with optical access, which allows

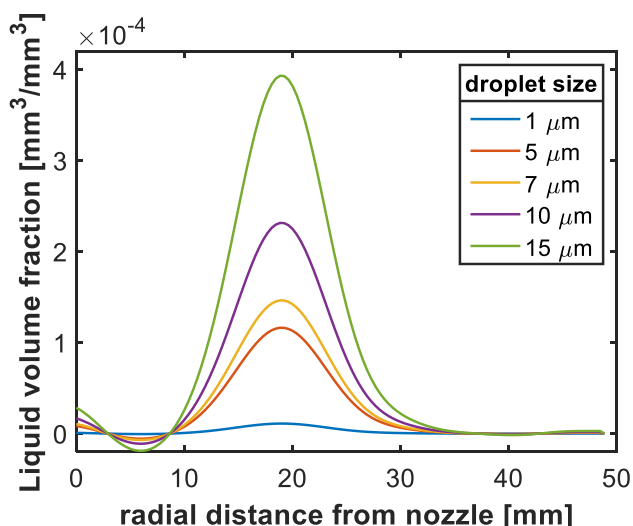


Fig. 14 Droplet size dependency on LVF results leads to uncertainties for quantification. PDI measurements in the ECN network show a droplet size distribution of 7 μm in the relevant spray regions, as discussed in a previous section

the investigation of different operation points instead of being limited to ambient conditions, unlike many other tomographic approaches. Unfortunately, the optical access of such a facility is not unlimited. Two main concerns that must be addressed are “windowing” and schlieren or “beam-steering” effects.

Windowing affects the tomographic reconstruction algorithm, where a circular data set, cropped by the circular windows of the chamber, is transferred to a cuboid three-dimensional space. Figure 15 shows that vignetting of the data appears, if the effective spray umbrella radius is bigger than the window radius and where it exceeds the window edges. Where this occurs, the front region of the dotted case in Fig. 15 cannot be properly reconstructed even though the middle plumes are fully captured. Essentially, all liquid in the spray must be contained in a given axial distance vertical slice, which was the method utilized in this study.

Another effect concerning window apertures is a potential sensitivity to beam-steering or schlieren effects that are problematic close to the edge of windows. Even in the center of the window, the quantification of DBIEI data is based on the assumption that schlieren effects are fully suppressed and that attenuation of the incoming light is only a result of Mie scatter/extinction effects. When using collimated lighting such as a single laser beam, one must use collection optics such as integrating spheres to accommodate the vapor-phase steering of the beam, which easily exceeds 100 mrad at high-pressure engine conditions (Musculus and Pickett 2005). As explained in the setup and in Ref. (Westlye et al. 2017), for the imaging setup, an engineered diffuser is utilized to produce a ray bundle over

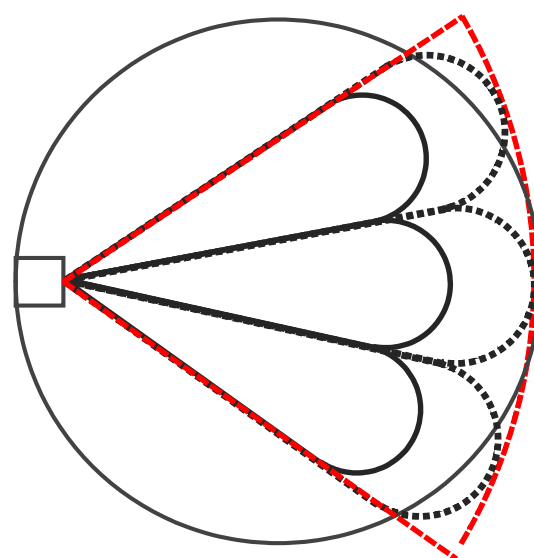


Fig. 15 The windowing effect: The effective spray umbrella has a bigger radius than the window and exceeds the window edges. The front region of the dotted case cannot be properly reconstructed anymore

a certain angle. This angle depends on the overall dimensions of the optical setup as illustrated in Fig. 9b (Westlye et al. 2017), with parameters for the current setup given in the embedded table. The “schlieren-free” image zone S does not extend all of the way to the window edge but depends upon a given DBIEI setup.

In a given setup, S depends on the assumption of the expected full beam-steering angle ζ , the diffuser diameter D , the distance from diffuser to the object plane L and the maximum collection angle of the system α_{\max} :

$$S \leq D - 2 \tan(\alpha_{\max} + \zeta) \cdot L, \tag{8}$$

$$\alpha_{\max} = \tan^{-1} \left(\frac{0.5(D + A_{\text{eff}})}{Q + L} \right). \tag{9}$$

The value for 2ζ has been evaluated in a high-pressure combustion system (Musculus and Pickett 2005) to be 2.86°. For evaporating gasoline sprays, this value is expected to be much smaller. Thus, the schlieren-free zone was calculated for 0.5° and 2.86° to be 79.9 mm and 73.0 mm, respectively. This means a reduction in workable area to only 63.92% and 58.40% of the full 125-mm window size.

8 Conclusion

This work introduces limited-view tomography to determine GDI plume directions in the three dimensions at high spatial and temporal resolution in a chamber at engine-relevant conditions. The results are based on extinction imaging measurements from three angles at speeds of 67.2 kHz. Using a projected liquid volume derived from Mie theory at the experiment collection angle and with previous measurements of droplet size (SMD, 7 μm), the CT reconstruction provides three-dimensional liquid volume fraction data that are used to identify the transient movement of each plume. The technique offers significant improvements compared to previous line-of-sight, planar or tomographic approaches for spray measurements.

To reduce time and data size for tomography, a minimum number of views are desired. Testing the method on synthetic model data, the reconstruction quality of 3- and 4-view-based inputs are compared to a full 180° input. The 3-view method leads to good average plume direction measurements for a symmetric 8-hole ECN Spray G injector, although the peak values in LVF are underestimated. Artifacts appear closer to the axis of symmetry in a magnitude of up to 20% of the peak value. The technique does not work for asymmetric spray patterns, such as spray with specific plumes directed at the spark plug.

The tomographic plume direction measurements of Spray G2 and G3 are robust against optically thick regions or droplet size uncertainties. Single plumes are distinct 5 mm downstream of the injector. X-ray tomography at Argonne National Lab provides the additional data closer to the nozzle for the same fuel injector (Duke et al. 2017). Uncertainties in the liquid volume fraction values are dependent on the utilization of limited views, as well as on droplet size. In the edge regions, windowing and schlieren effects have influence on the accuracy.

The optically measured plume directions are in good agreement with mechanical patterning data from Delphi. Even the trend of individual plume direction is similar. Plume-to-plume interactions reduce the plume direction angle in comparison to the drill-hole angle at G3 conditions, and even more at flash-boiling G2 conditions. These data form a valuable dataset for evaluating CFD models at the same conditions, which are ultimately used to improve engine design.

Acknowledgements Open Access funding provided by Projekt DEAL. We gratefully acknowledge the Bavaria California Technology Center (BaCaTec) and the School of Advanced Optical Technologies (SAOT) for supporting an international visiting program of Lukas Weiss at the Sandia National Laboratories. The authors also wish to thank G. Singh, M. Weismiller, and K. Stork, program managers at the U.S. DOE, for their support. We also thank L. Markle of Delphi for donation of the Spray G injector to the ECN and for the patterning

experimental data provided. Sandia National Laboratories is a multi-mission laboratory managed and operated by National Technology and Engineering Solutions of Sandia, LLC., a wholly owned subsidiary of Honeywell International, Inc., for the DOE's National Nuclear Security Administration under contract DE-NA0003525.

Open Access This article is licensed under a Creative Commons Attribution 4.0 International License, which permits use, sharing, adaptation, distribution and reproduction in any medium or format, as long as you give appropriate credit to the original author(s) and the source, provide a link to the Creative Commons licence, and indicate if changes were made. The images or other third party material in this article are included in the article's Creative Commons licence, unless indicated otherwise in a credit line to the material. If material is not included in the article's Creative Commons licence and your intended use is not permitted by statutory regulation or exceeds the permitted use, you will need to obtain permission directly from the copyright holder. To view a copy of this licence, visit <http://creativecommons.org/licenses/by/4.0/>.

References

- Berrocal E, Sedarsky DL, Paciaroni ME, Meglinski IV, Linne MA (2007) Laser light scattering in turbid media Part I: experimental and simulated results for the spatial intensity distribution. *Opt Express* 15(17):10649
- Berrocal E, Kristensson E, Richter M, Linne M, Alden M (2008) Multiple scattering suppression in planar laser imaging of dense sprays by means of structured illumination. *Opt Express* 16(22):17870–17881
- Berrocal E et al (2019) Two-photon fluorescence laser sheet imaging for high contrast visualization of atomizing sprays. *OSA Contin* 2(3):983
- Bieberle M et al (2009) Experimental two-phase flow measurement using ultra fast limited-angle-type electron beam X-ray computed tomography. *Exp Fluids* 47(3):369–378
- Bornschlegel S, Conrad C, Eichhorn L, Wensing M (2017) Flashboiling atomization in nozzles for GDI engines. In: ILASS—Europe 2017
- Duke DJ et al (2015) Time-resolved X-ray tomography of gasoline direct injection sprays. *SAE Int J Engines* 9:143
- Duke DJ et al (2017) Internal and near nozzle measurements of Engine Combustion Network ‘Spray G’ gasoline direct injectors. *Exp Therm Fluid Sci* 88(June):608–621
- ECN (2019) “Primary Spray G dataset,” ECN webpage. [Online]. Available: <https://ecn.sandia.gov/gasoline-spray-combustion/target-condition/primary-spray-g-datasets/>. Accessed 20 Sep 2019
- “En’Urga Inc.,” “SETscan OP-400 brochure,” <https://www.enurga.com>. [Online]. Available: https://www.enurga.com/assets/docs/OP-400_brochure.pdf. Accessed 09 Sep 2019
- Engine Combustion Network (2018) “ECN 6 workshop,” ECN webpage, 2018. [Online]. Available: <https://ecn.sandia.gov/ecn-works-hop/ecn6-workshop/>
- Engine Combustion Network (2019) “ECN Spray G target conditions,” ECN webpage, 2019. [Online]. Available: <https://ecn.sandia.gov/gasoline-spray-combustion/target-condition/spray-g-operating-condition/>
- Heldmann M, Bornschlegel S, Wensing M (2015) Investigation of jet-to-jet interaction in sprays for DISI engines. *SAE Tech. Pap.* 2015-01-1899
- Kak AC, Slaney M, Wang G (2002) Principles of computerized tomographic imaging. *Med Phys* 29(1):107

- Kim T, Park S (2006) Effects of spray patterns on the mixture formation process in multi-hole-type direct injection spark ignition (DISI) gasoline engines. *At Sprays* 26(11):1151
- Klinner J, Willert C (2012) Tomographic shadowgraphy for three-dimensional reconstruction of instantaneous spray distributions. *Exp Fluids* 53(2):531–543
- Lim J, Sivathanu Y, Wolverson M, Green J (2018) Conversion of scattering phase function to SMD in scattering/extinction tomography. ICLASS 2018, vol 14th Trien, no. August, pp 1–7
- Manin J, Skeen SA, Pickett LM, Parrish SE, Markle LE (2015) Experimental characterization of DI gasoline injection processes. SAE Tech. Pap. 2015-01-1894
- McMackin L, Hugo RJ, Bishop KP, Chen EY, Pierson RE, Truman CR (1999) High speed optical tomography system for quantitative measurement and visualization of dynamic features in a round jet. *Exp Fluids* 26(3):249–256
- Musculus MPB, Kattke K (2010) Entrainment Waves in Diesel Jets. *SAE Int J Engines* 2(1):1170–1193
- Musculus MPB, Kattke K (2019) One-dimensional control-volume jet model.” ECN webpage, 2019. [Online]. Available: <https://ecn.sandia.gov/diesel-spray-combustion/computational-method/one-dimensional-control-volume-jet-model/>
- Musculus MPB, Pickett LM (2005) Diagnostic considerations for optical laser-extinction measurements of soot in high-pressure transient combustion environments. *Combust Flame* 141(4):371–391
- Parrish SE (2014) Evaluation of liquid and vapor penetration of sprays from a multi-hole gasoline fuel injector operating under engine-like conditions. *SAE Int J Engines* 7(2):1017–1033
- Parrish SE, Zink RJ, Sivathanu YR, Lim J (2010) Spray patterning of a multi-hole injector utilizing planar line-of-sight extinction tomography. In: ICLASS Americans 22nd annual conference of the institute for liquid atomization and spray systems, pp 1–10
- Payri R, Salvador FJ, Martí-Aldaraví P, Vaquerizo D (2017) ECN Spray G external spray visualization and spray collapse description through penetration and morphology analysis. *Appl Therm Eng* 112:304–316
- Peterson B, Sick V (2009) Simultaneous flow field and fuel concentration imaging at 4.8 kHz in an operating engine. *Appl Phys B Lasers Opt* 97(4):887–895
- Pickett LM, Genzale CL, Manin J (2015) Uncertainty quantification for liquid penetration of evaporating sprays at diesel-like conditions. *At Sprays* 25(5):425
- SAE (2007) J2715—Gasoline fuel injector spray measurement and characterization
- Sphicas P, Pickett LM, Skeen SA, Frank JH (2017) Inter-plume aerodynamics for gasoline spray collapse. *Int J Engine Res* 19(10):1048–1067
- Sphicas P, Skeen SA, Parrish S, Frank JH, Pickett LM (2018) Inter-plume velocity and extinction imaging measurements to understand spray collapse when varying injection duration or number of injections. *At Sprays* 28(9):837–856
- Spiegel L, Spicher U (2010) Mixture formation and combustion in a spark ignition engine with direct fuel injection. *SAE Trans* 920521:967–975
- Storch M et al (2016) Two-phase SLIPI for instantaneous LIF and Mie imaging of transient fuel sprays. *Opt Lett* 41(23):5422
- Westlye FR, Penney K, Ivarsson A, Pickett LM, Manin J, Skeen SA (2017) Diffuse back-illumination setup for high temporally resolved extinction imaging. *Appl Opt* 56(17):5028
- Zhao H (2009) Advanced direct injection combustion engine technologies and development: diesel engines, vol 2. Elsevier, Amsterdam

Publisher's Note Springer Nature remains neutral with regard to jurisdictional claims in published maps and institutional affiliations.